Dynamics of a distorted diamond chain

H.-J. Mikeska and C. Luckmann
Institut für Theoretische Physik, Universität Hannover, 30167 Hannover, Germany
(Received 26 September 2007; revised manuscript received 7 January 2008; published 6 February 2008)

We present results on the dynamics of the distorted diamond chain, $S=1/2$ dimers alternating with single spins 1/2 and exchange couplings J_1 and J_3 in between. The dynamics in the spin fluid (SF) and tetramer-dimer (TD) phases is investigated numerically by exact diagonalization for up to 24 spins. Representative excitation spectra are presented both for zero magnetic field and in the 1/3 plateau phase and the relevant parameters are determined across the phase diagram. The behavior across the SF-TD phase transition line is discussed for the specific heat and for excitation spectra. The relevance of the distorted diamond chain model for the $Cu_3(CO_3)_2(OH)_2$ (azurite) material is discussed with particular emphasis on inelastic neutron scattering experiments; the recent suggestion of one possibly ferromagnetic coupling constant is not confirmed.

DOI: 10.1103/PhysRevB.77.054405 PACS number(s): 75.10.Jm, 75.10.Pq, 75.40.Gb

I. INTRODUCTION

The distorted diamond chain (DDC) is a one-dimensional quantum spin model with structure as shown in Fig. 1(a) and Hamiltonian

$$H=\sum_{n=1}^{N/3}\{J_2\mathbf{S}_{3n+1}\mathbf{S}_{3n+2}+J_1(\mathbf{S}_{3n}\mathbf{S}_{3n+1}+\mathbf{S}_{3n+2}\mathbf{S}_{3n+3}) + J_3(\mathbf{S}_{3n}\mathbf{S}_{3n+2}+\mathbf{S}_{3n+1}\mathbf{S}_{3n+3})\}. \quad (1)$$

This model with spins 1/2 and all antiferromagnetic couplings may be strongly frustrated owing to the triangular building blocks and has received increasing theoretical[1–7] as well as experimental[8–10] interest in the past decade for a number of reasons: It has a rich quantum phase diagram as shown in Fig. 1(b) (taken from Ref. 3). Here and in the following, we choose a representation with $J_2=1$ as energy unit and J_1,J_3 as variables. This representation emphasizes the symmetry of the model under exchange of J_1 and J_3. Three quantum phases have been discussed for the ground state of the model in zero magnetic field. For $J_1,J_3\ll 1$, the ground state develops from the state with dimers in their singlet state on J_2 bonds and nearly free spins between these dimers. The low energy sector is governed by an effective one-dimensional Heisenberg antiferromagnetic (HAF) with $N/3$ sites resulting from the residual coupling between these spins and denoted as J_{eff} in the following. This leads to the formation of a spin fluid (SF) phase with additional high energy excitations. For intermediate J_1,J_3, the ground state dimerizes, forming a twofold degenerate sequence of alternating tetramers and dimers (TD phase). Finally, for both J_1,J_3 sufficiently large, the ground state is ferrimagnetic with, e.g., a $\uparrow\uparrow\downarrow$ structure in the unit cell of three spins (which satisfies J_1 and J_3 bonds and frustrates J_2). These three phases can be clearly identified already in the symmetric model with $J_1=J_3$ in the regimes $J_1=J_3\leqslant 1/2$ (SF phase), $1/2\leqslant J_1=J_3\leqslant J_m$ (TD phase), and $J_m\leqslant J_1=J_3$ (ferrimagnetic phase) with $J_m\approx 1.10$.[1]

The generalization to the distorted diamond chain $J_1\neq J_3$ leads to an even richer behavior including, e.g., the trimer Heisenberg antiferromagnetic chain on the $J_3=0$ axis with the standard HAF for $J_1=1$ as limiting case. The DDC model can be seen as generalization of the HAF with nearest neighbor and next nearest neighbor interactions: The critical point of this model at $J_{\mathrm{NNN}}/J_{\mathrm{NN}}\approx 0.2411$,[11] which marks the transition from a spin fluid to the dimerized phase, is extended into the line between the SF and the TD phases in the DDC model and the Majumdar-Ghosh point at $J_{\mathrm{NNN}}/J_{\mathrm{NN}}=1/2$ is extended into the line $1/2\leqslant J_1=J_3\leqslant J_m$ with simple and exactly known dimerized ground states. In particular, the transition line between the SF and TD phases is a line of Kosterlitz-Thouless phase transitions. The point $J_1=J_3=1/2$ is a point of particular high degeneracy. However, compared to the simple HAF chain with nearest and next-nearest neighbor exchange, the DDC model has the dimer subsystem as an additional degree of freedom which dominates the high energy regime, but also, in the appropriate parameter regime, interacts with the low energy spin part. The ferrimagnetic part of the quantum phase diagram is another consequence of the combined influence of these 2 degrees of freedom. In

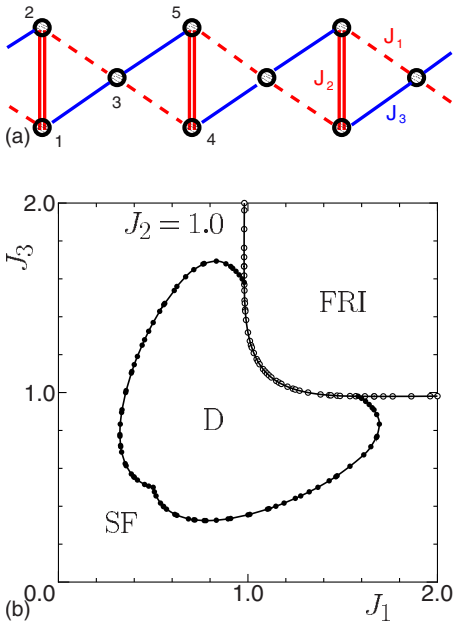

FIG. 1. (Color online) (a) Structure and (b) phase diagram of the distorted diamond chain model [(b) from Ref. 3].

addition to the ideal DDC as defined in Eq. (1), models with somewhat modified interactions, such as the tetrahedron chain[12] and the strongly anisotropic xy version of the DDC,[13] have been considered and serve to illustrate the effect of deviating from the ideal isotropic diamond structure.

An external magnetic field polarizes the quasi-free-spins and at a critical field H_{c1} produces a magnetization plateau at $1/3$ of the total saturation magnetization. The plateau state corresponds to a fully saturated subsystem of spins $1/2$ and all dimers (J_2 bonds) in their singlet state. Further increase of the moment requires breaking up at least one dimer with its large energy scale $J_2=1$, and therefore a correspondingly higher field $H \geqslant H_{c2}$ (end of the plateau). Finally, complete saturation is obtained at the field H_{sat}, given by

$$\frac{H_{\mathrm{sat}}}{J_2} = \frac{1}{2} + \frac{3}{4}(J_1 + J_3) + \frac{1}{2}\left\{ 2(J_1 - J_3)^2 + \frac{1}{4}(J_1 + J_3)^2 + 1 - (J_1 + J_3) \right\}^{1/2}. \tag{2}$$

The critical field H_{c1} (beginning of the $1/3$ plateau) is determined by the level crossing between the saturated state of the effective HAF and its "ferromagnon" excitation with one unit of magnetization less. If the mapping to the effective HAF applies, this gives the relation

$$H_{c1} = 2J_{\mathrm{eff}}. \tag{3}$$

Apart from the theoretical interest in investigating a model which allows to follow the variation between different quantum phases, the DDC model is of interest since it seems to describe reasonably well the compound azurite, $Cu_3(CO_3)_2(OH)_2$. Azurite has been investigated in detail by high field electron spin resonance,[8] as well as by static measurements (magnetization, susceptibility, specific heat),[9] and the existence of the $1/3$ magnetization plateau has been clearly established. From these experiments, this compound appears to be in the SF phase close to the phase transition to the TD phase. Recently, however, the possibility of one of the couplings J_1, J_3 being ferromagnetic has been suggested from susceptibility and specific heat data.[6,14] Beyond the static properties investigated so far, the dynamics of the DDC and the material azurite, in particular, remain as a challenge to be understood both experimentally and theoretically. The characteristic feature of the model, namely, the presence of 2 degrees of freedom with different energy scales and their mutual influence will show up most clearly in the energy spectra of the model. These are best investigated by inelastic neutron scattering (INS) experiments as clearly seen in a recent work.[10] For a more complete description of both the DDC in the full phase diagram and the results of INS experiments on azurite, we present in the following results on the dynamics in the SF phase (Sec. II) and in the TD phase (Sec. III).

A perturbative approach can be applied to obtain results in the regime $J_1, J_3 \ll 1$ (see Ref. 4) as well as close to some special points in the phase diagram. Generally, however, for a quantitative description, numerical calculations are required. We will present in the following the results of exact diagonalization using both the Lanczos algorithm for systems with 24 spins and complete diagonalization (all eigenvalues) for 12 and 18 spins. The latter are necessary since the Lanczos algorithm gives only a limited number of the lowest energy levels in the subspace considered (in our case, S^z_{tot} and wave vector k), which is not sufficient to cover the excited dimer subspace with its higher energies. Since the elementary cell has three spins, our system sizes are restricted to four, six, and eight elementary cells. It turns out, however, that for many aspects, this is sufficient to obtain reliable results for the infinite system when a finite size analysis is carried through.

II. DYNAMICS IN THE SPIN FLUID PHASE

It is helpful to start the discussion from two well known limiting cases:

(i) For $J_1=J_3=0$, the system reduces to $N/3$ independent dimers and $N/3$ free spins. In the ground state, all dimers are in their singlet state and a $2^{N/3}$-fold degeneracy due to the free spins results. A magnetic field immediately saturates the free spin system leading to a magnetization of $M_{\mathrm{sat}}/3$ which remains constant until, at a field $H_{c2}=J_2$, the dimers change to their triplet states saturating the system. This behavior to a certain extent remains valid on the symmetry line $J_1=J_3$ where the total spin on all J_2 bonds is independently conserved. The ground state, as well as the $1/3$ magnetization plateau in the low field, remains unchanged, whereas the transition to full saturation is determined by the effective interaction which develops between two neighboring dimers in their triplet state and finally leads to an effective $S=1$ chain. Qualitatively, for a large range of parameters, the distorted diamond chain can be divided into two subsystems with clearly different energy scales, a low energy part of $N/3$ spins $1/2$ and a high energy part of $N/3$ dimers.

For small deviations from the independent free spin limit, $J_1 \neq J_3$, the spin $1/2$ subsystem develops some coupling by polarizing intermediate dimers and the $2^{N/3}$-fold degeneracy is lifted in favor of an effective Heisenberg chain with exchange J_{eff}. In this regime, excitations of the DDC remain well separated. They are in the low energy regime with energy scale J_{eff} forming the spinon continuum of the HAF with $N/3$ spins in the Brillouin zone of the full DDC (lattice constant a, reciprocal lattice vector $\tau=2\pi/a$) or in the high energy regime with energy scale $J_2=1$ corresponding to the excitation of a dimer to its triplet state and developing into a dispersive band with width Δ_{dimer} due to the coupling to the low energy spin subsystem. We will not consider states with more than one excited dimer in the following.

(ii) For $J_1=1, J_3=0$, the system reduces to the Heisenberg antiferromagnet with N spins, forming a spinon continuum in the Brillouin cell with reciprocal lattice vector 3τ, energy scale 1, and no additional high energy excitations. For $0 < J_1 < 1$, we have a trimerized Heisenberg chain and the spectrum is obtained by folding back the spinon continuum to the smaller Brillouin zone corresponding to lattice constant a. This results in three excitation branches (actually continua) which fill the energy range up to $\epsilon=\pi$ with small

(for J_1 slightly less then 1) gaps between them and an alternating sequence of minimum, maximum, and minimum at wave vector $k=\pi$ (in the following, we will use exclusively the Brillouin zone with reciprocal lattice vector τ, corresponding to the full DDC). With increasing $1-J_1$, these trimer bands develop increasingly larger gaps; finally, the continuum of the effective HAF emerges from the lowest band and the two upper bands conspire to give the dimer excitations decorated by continua of low energy spinon excitations.

Using this frame, the lowest excitations of interest in the following are easily described:

(i) the spinon continuum of the effective chain,

(ii) the band with one excited dimer above the spinon continuum,

(iii) the "inverted ferromagnon," i.e., the saturated effective HAF with one spin deviation $\left(S^z_{\mathrm{tot}}=\frac{1}{2}N/3-1\right)$, and

(iv) the band with one excited dimer above the saturated effective HAF, i.e., one dimer in its triplet state $\left(S^z_{\mathrm{tot}}=\frac{1}{2}N/3+1\right)$.

The dispersion of excitations (ii)–(iv) is determined by hopping processes (spin deviations and dimer triplets, respectively, moving to neighboring sites due to the residual interactions). To lowest order, these processes result in a cosine dispersion and we introduce the following as notation for (ii):

$$\epsilon^{(0)}_{\mathrm{dimer}}(k)=1+\delta^{(0)}_{\mathrm{dimer}}+\frac{1}{2}\Delta^{(0)}_{\mathrm{dimer}}\cos k. \tag{4}$$

More precisely, this excitation is not a single band but a continuum due to the spinon continuum of initial states; however, we will only be able to discuss the lower edge of this excitation and therefore simplify the notation using Eq. (4). Excitations (iii) and (iv) are the relevant excitations above the 1/3 plateau; we therefore use a notation giving their energies in finite magnetic fields relative to the plateau ground state with $S^z_{\mathrm{tot}}=\frac{1}{2}N/3$:

$$\epsilon_{\mathrm{ferrom}}(k)=\frac{1}{2}\Delta_{\mathrm{ferrom}}(1+\cos k)+H-H_{c1}, \tag{5}$$

$$\epsilon^{(\mathrm{sat})}_{\mathrm{dimer}}(k)=1+\frac{1}{2}(J_1+J_3)+\delta^{(\mathrm{sat})}_{\mathrm{dimer}}+\frac{1}{2}\Delta^{(\mathrm{sat})}_{\mathrm{dimer}}(1+\cos k)-(H-H_{c1}). \tag{6}$$

The quantities Δ and δ give the widths and the nontrivial contributions, respectively, to the minimum energy (at $k=\pi$) of the corresponding bands. The cosine dispersion, of course, is only valid in lowest order and will change to a more complicated expression for real systems.

In the model of an effective HAF for the low energy regime, its exchange constant J_{eff} determines the low energy spinon (i) and the inverted ferromagnon spectrum: $\Delta_{\mathrm{ferrom}}=2J_{\mathrm{eff}}$. Combined with $\epsilon^{(\mathrm{sat})}_{\mathrm{dimer}}$, it is also sufficient to give the range of the plateau phase and to characterize its dynamics: In the presence of a finite field, spectra are identical to those without field except for the shifts and splittings due to Zeeman energies. This establishes states with an increasingly larger total spin S_{tot} (in their maximum z component) as ground states. The plateau begins at the field H_{c1} when the $S_{\mathrm{tot}}=\frac{1}{2}N/3$ level (saturated state of the quasi-free-spin subsystem) is forced below the lowest $S_{\mathrm{tot}}=\frac{1}{2}N/3-1$ level (ferromagnon band at wave vector π) by the external field, leading to $H_{c1}=2J_{\mathrm{eff}}$. The lowest excitation for the plateau dynamics close to the field H_{c1} then is the ferromagnon of Eq. (5). When the field is increased across the plateau regime, the $S_{\mathrm{tot}}=\frac{1}{2}N/3+1$ level (one excited dimer on top of the saturated quasi-free-spin subsystem) lowers its energy, crosses the ferromagnon excitation, and, finally, is responsible for the end of the plateau at the upper plateau field H_{c2} implying

$$H_{c2}=H_{c1}+1+\frac{1}{2}(J_1+J_3)+\delta^{\mathrm{sat}}_{\mathrm{dimer}}. \tag{7}$$

The parameters determining the spectra can be calculated in perturbation theory in J_1,J_3 and to lowest order are determined by the level spectrum of the general ($J_1\neq J_3$) tetramer with four spins 0,…,3. This spectrum includes the lowest order information about J_{eff} in the singlet-triplet splitting of spins 0 and 3 and about $\Delta^{(\mathrm{sat})}_{\mathrm{dimer}}$ in the amplitude for the process $|\uparrow s\rangle\rightarrow|\downarrow t_{\pm}\rangle$ (s and t_+ are noninteracting dimer states) which determines the propagation of an excited dimer triplet. The results to lowest order in J_1,J_3 are

$$2J_{\mathrm{eff}}=\Delta_{\mathrm{ferrom}}=2\Delta^{\mathrm{sat}}_{\mathrm{dimer}}=(J_1-J_3)^2,$$

$$\delta^{\mathrm{sat}}_{\mathrm{dimer}}=-(J_1-J_3)^2,$$

$$H_{c2}=1+\frac{1}{2}(J_1+J_3). \tag{8}$$

J_{eff} has been calculated in straightforward perturbation theory up to fifth order.[4] Based on the splitting of the general tetramer into singlet and triplet states, we have obtained a result which accounts partly also for higher orders and allows reasonable estimates for $|J_1-J_3|\ll 1$ but finite J_1+J_3:

$$J_{\mathrm{eff}}=\frac{1}{2}\{\{(J_1+J_3-1)^2+3(J_1-J_3)^2\}^{1/2}+J_1+J_3-\{1+(J_1-J_3)^2\}^{1/2}\}. \tag{9}$$

In lowest order perturbation theory, the relevant parameter, in addition to the energy scale set by J_2 and to J_1+J_3, is the exchange of the effective HAF determined by $(J_1-J_3)^2$ and many characteristic quantities of the DDC would be related by simple numerical factors if the mapping were perfect. Whereas these perturbational results allow us to discuss the dynamics in principle, J_1,J_3 values of interest for the bulk of the phase diagram as well as for a material such as azurite are beyond the validity of perturbation theory. We therefore present in the following results from the numerical approaches described above. This will allow us to follow the essential aspects of the dynamics in the intermediate regime, i.e., through all of the SF phase. In Figs. 2 and 3, we show excitation spectra for a representative sequence of three sets of exchange parameters: set (a) represents the case of small couplings, set (b) is for a point in the phase diagram close to

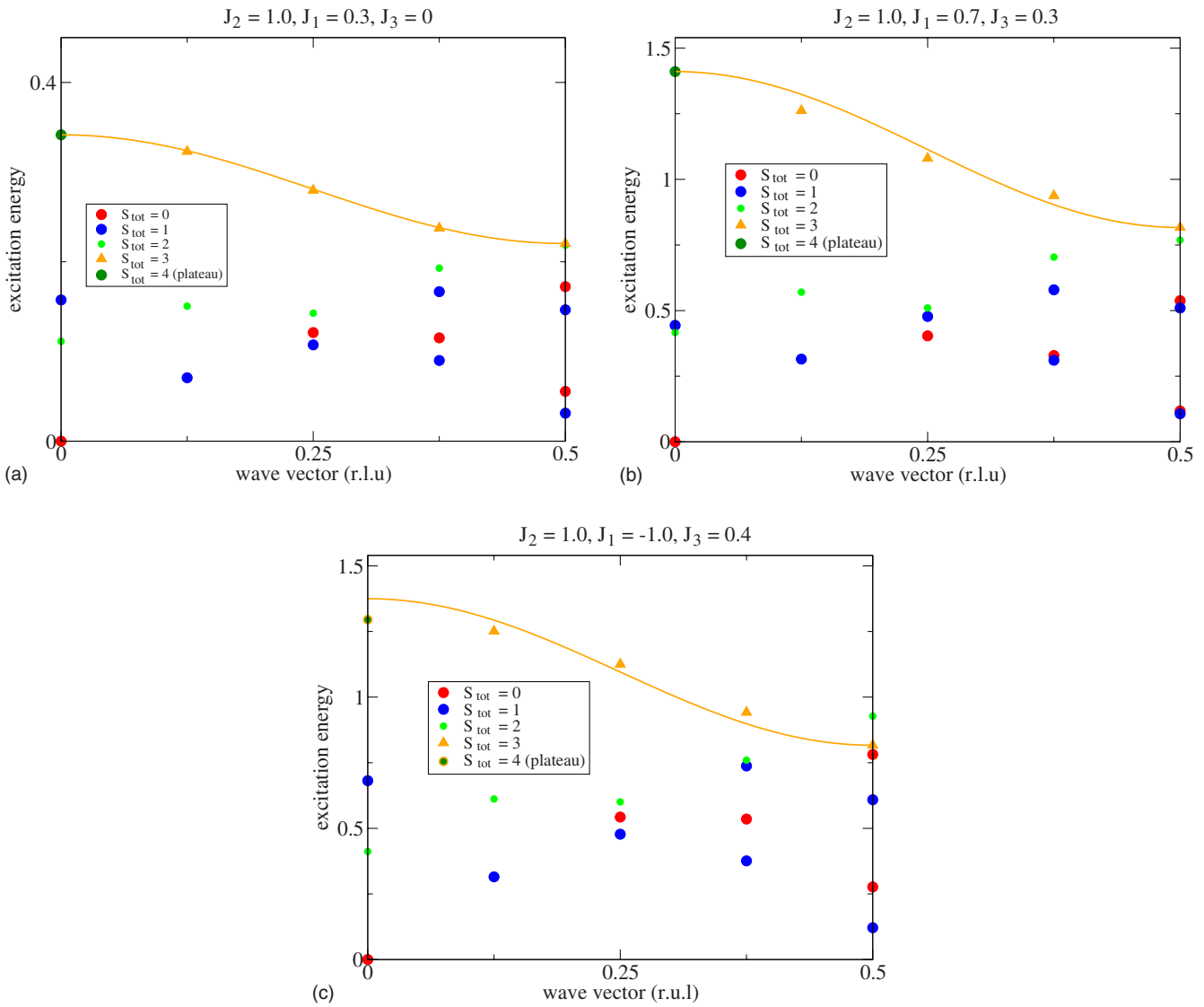

FIG. 2. (Color online) Low energy spectrum of the DDC for $N=24$, $H=0$, $J_2=1.0$ and (a) $J_1=0.3$, $J_3=0$, (b) $J_1=0.7$, $J_3=0.3$, and (c) $J_1=-1.0$, $J_3=0.4$.

the SF to TD transition thought to be qualitatively representative for azurite,[9] and set (c) shows results for the case of one coupling ferromagnetic. The data are obtained by diagonalizing chains with 24 spins using the Lanczos algorithm.

The low energy excitation spectra in zero external field are shown in Fig. 2. Here and in the following, energies are in units of J_2 and wave vectors in reciprocal lattice units (shown is the interval $k=0,\ldots,\pi$, corresponding to half of the Brillouin zone). The spectra include all levels with $S_{\mathrm{tot}}=0,1$ of the spinon type in the low energy subsystem of eight spins and, in addition, the lowest excitations for $S_{\mathrm{tot}}=2$ (for completeness) and $S_{\mathrm{tot}}=3$. The latter band of excitations is the inverted ferromagnon and a cosine dispersion approximating the data points is shown for qualitative comparison to the effective model with its exact cosine dispersion. Figure 3 shows the excitation bands in a magnetic field H_{c1} (beginning of the 1/3 plateau). In magnetic field, two Zeeman components of the $S_{\mathrm{tot}}=4$, $k=0$ level are relevant: The $S^z_{\mathrm{tot}}=4$ component turns into the plateau ground state, whereas the $S^z_{\mathrm{tot}}=3$ component becomes the top of the inverted ferromagnon band. It is identical to that of Fig. 2 (apart from Zeeman shift) and now the lowest excitation. In addition, Fig. 3 shows the lowest excitation band with $S_{\mathrm{tot}}=5$, which requires breaking one dimer (J_2) bond. Cosine dispersions as approximation to the data points are included for these two bands. For completeness, we also show the first full band with $S_{\mathrm{tot}}=4$ above the plateau ground state.

Among the data shown, the excitations of interest from an experimental point of view (with large transition matrix elements for, e.g., INS) are the spinon continuum in zero field and the inverted ferromagnon band, as well as the excited dimer band in the plateau field. In addition, in zero field, there will be transitions with energy of the order of J_2 to an excited dimer band with $S_{\mathrm{tot}}=1$ resulting from breaking a J_2 bond on top of the effective chain ground state. This is more difficult to deal with than the excited dimer excitation shown in Fig. 3, which is on top of the less complex saturated effective chain state. We will discuss these excitations below

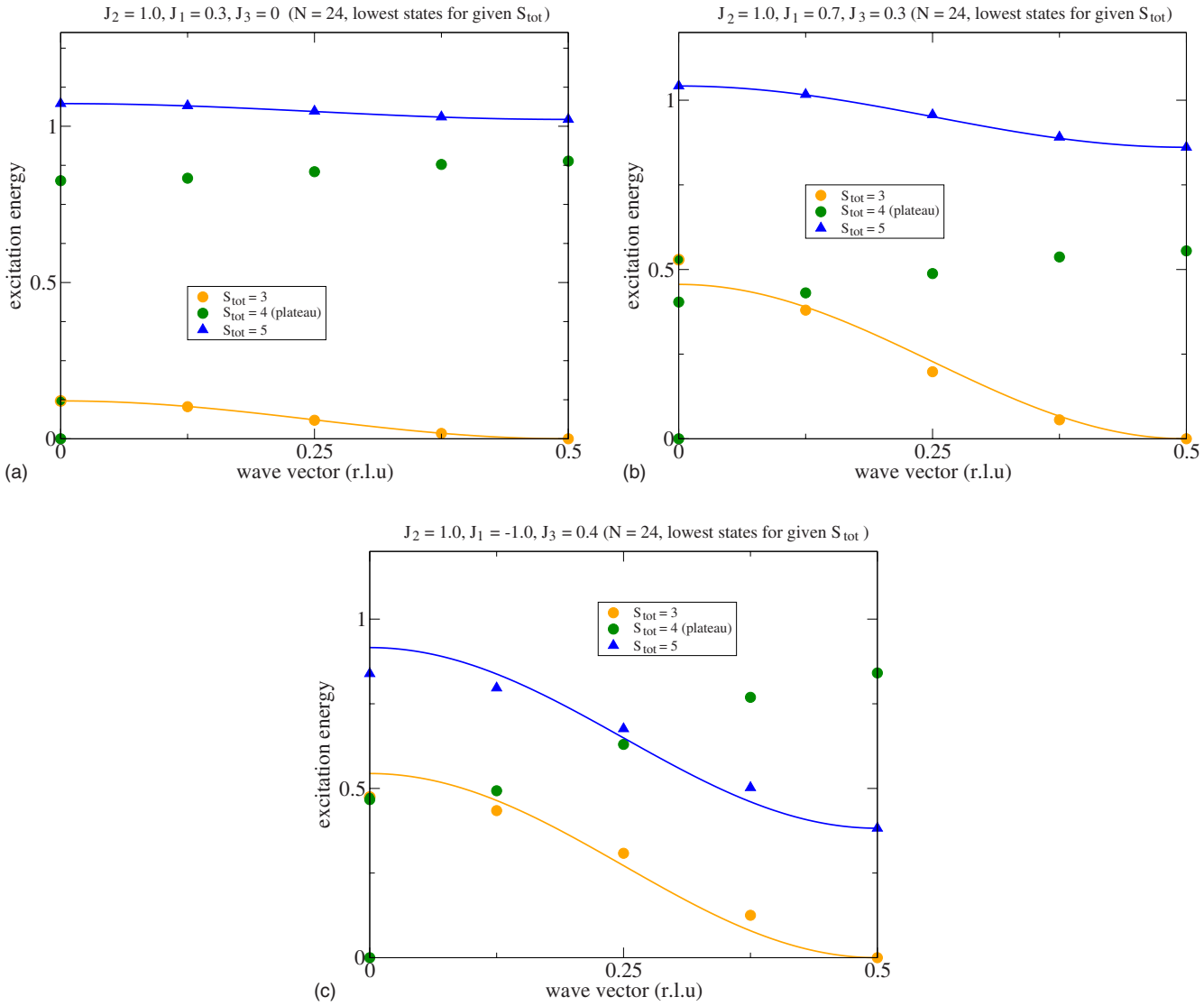

FIG. 3. (Color online) Excitation spectrum of the DDC above the 1/3 plateau for $N=24$, $H=H_{c1}$, $J_2=1.0$ and (a) $J_1=0.3$, $J_3=0$, (b) $J_1=0.7$, $J_3=0.3$, and (c) $J_1=-1.0$, $J_3=0.4$.

based on calculations of all eigenvalues of an $N=18$ chain (see Table III). States with $S_{\mathrm{tot}}>1$ in zero field, as well as the band with $S_{\mathrm{tot}}=4$ above the plateau ground state, will be only weakly excited in INS and analogous experiments. In particular, states in the $S_{\mathrm{tot}}=4$ band are obtained from the saturated state by the virtual excitation $|s\uparrow\rangle \rightarrow |t_+\downarrow\rangle$. They have an excited dimer *and* an overturned spin (compared to the saturated state) in the low energy subsystem and thus require two spin flips to be excited.

We now discuss how the dynamics changes with varying exchange constants. Set (a) shows the behavior typical for the weakly coupled DDC: the bands are well separated in energy and the cosine dispersion is nearly perfect. Set (b) displays what is expected qualitatively for a material such as azurite: in zero field, a spinon continuum should be clearly visible, whereas in the plateau regime, two separate bands dominate the picture. The cosine approximation to the dispersion is less applicable. Actually, the spectrum of the inverted ferromagnon is close to linear for smaller wave vectors. For set (c), which serves as an example for the alternative suggesting one ferromagnetic coupling,[6,14] the dynamics in zero field is seen to be surprisingly close to that of set (a). This may explain the emergence of the ferromagnetic alternative from a discussion of static quantities. However, these two sets lead to strongly differing dynamics in finite field, as seen by comparing Figs. 3(b) and 3(c). The standard antiferromagnetic model (b) implies two well separated bands with rather small widths, whereas the partly ferromagnetic alternative (c) is characterized by an overlap of the two bands and a strong dispersion of the excited dimer band.

For a semiquantitative discussion of the low energy dynamics of the DDC, the mapping to the model of an effective HAF is rather useful. Therefore, we discuss shortly the quality of this mapping for $H=0$ in Fig. 4 for the two parameter sets (a) $J_1=0.3$, $J_3=0$ and (b) $J_1=0.7$, $J_3=0.3$. We compare the numerical spectrum for $N=24$ (dots) with the energies of the $N=8$ HAF with unity exchange constant (open circles). The energies of the DDC have been scaled by an effective

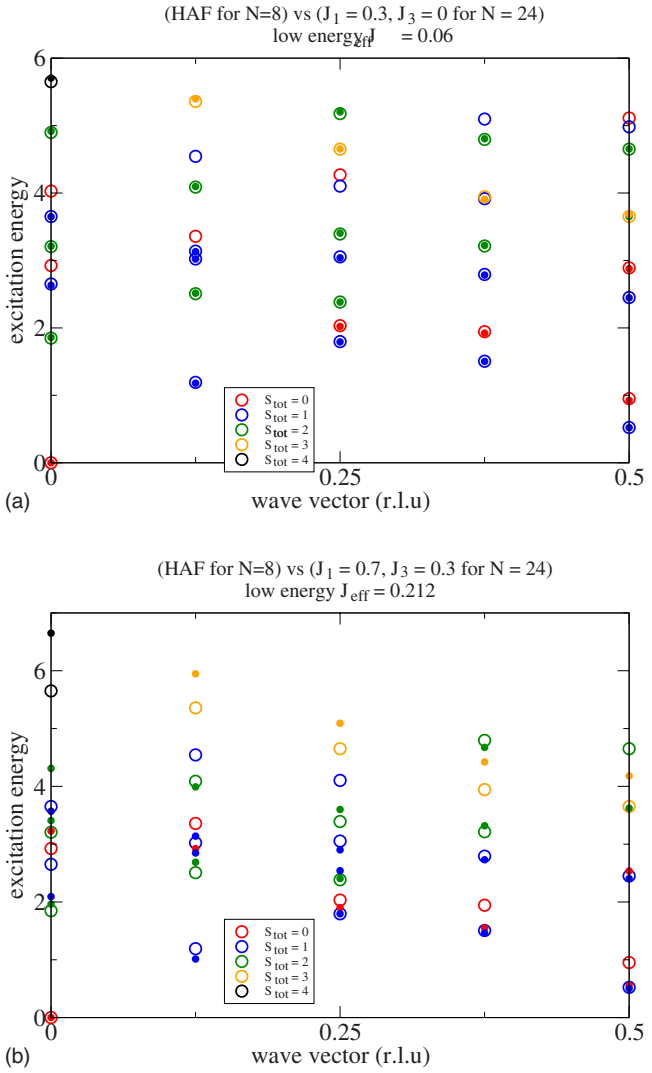

FIG. 4. (Color online) Spectrum of the effective HAF ($N=8$) vs spectrum of the DDC for $N=24$, $H=0$, $J_2=1$ and (a) $J_1=0.3$, $J_3=0$ and (b) $J_1=0.7$, $J_3=0.3$ (see text).

exchange constant J_{eff}, chosen to reproduce the ($N=8$) maximum spinon energy at $k=\frac{\pi}{2}$, $S_{\text{tot}}=1$. For the parameter set (b), energy levels of the $N=8$ HAF, which are beyond the range of the Lanczos calculation for the DDC model, have been omitted from the plot to obtain a clearer picture. Whereas the mapping for the small coupling constants of set (a) is nearly perfect throughout all of the spectrum, substantial deviations are seen for the parameter set (b): the low energy spinon part is still reproduced well by the effective model, but the high energy part, in particular, the ferromagnon band with $S_{\text{tot}}=3$, is very different both in energy and in dispersion. A cosine dispersion is only a rough approximation to the spectrum.

Thus, a quantitative experimental investigation of the dynamics will contribute substantially to locating the position of a specific compound in the phase diagram of Fig. 1(b). For a quantitative overview (and possibly for use in the determination of coupling parameters from experiment), we discuss in the following the characteristics of the spectra for a wider range of exchange coupling constants. In Tables I and II below, we present the information obtained from the numerical calculations after reducing the spectral data to a few characteristic numbers. First, from the numerical data, we have calculated values for the quantities determined by the effective exchange between the quasi-free-spins. In table I, we give numbers for J_{eff} determined from the maximum spinon energy at $k=\pi/2$, $S_{\text{tot}}=1$ (when multiplied by $1.7964\cdots$, the corresponding energy in the $N=8$ HAF chain, these numbers lead back to the energy for the DDC model) and for the $S_{\text{tot}}=1$ spinon at $k=\pi$ (gapped due to discreteness). Further, we give the width of the ferromagnon band (which would be $2J_{\text{eff}}$ if the mapping to the effective model were perfect) and the width of the dimer band above the plateau with $S_{\text{tot}}=N/6+1$. In Table II, we give numerical values for the characteristic magnetic fields, i.e., beginning (H_{c1}) and end (H_{c2}) of the plateau, as well as the saturation field H_{sat}. In the standard case (actually, some exceptions exist close to the phase transition line), H_{c1} is identical to the ferromagnon width from Table I. In Table II, we also give the energy scale

TABLE I. DDC parameters related to the effective interaction (see text).

Couplings J_1, J_3	J_{eff} from spinon maximum	J_{eff} from spinon at $k=\pi$	Ferromagnon Width	Dimer band width
0.02, 0.00	2.06×10^{-3}	2.06×10^{-3}	4.12×10^{-3}	2.02×10^{-3}
0.30, 0.00	0.060	0.060	0.121	0.051
0.60, 0.00	0.223	0.207	0.480	0.218
0.80, 0.00	0.343	0.291	0.795	0.400
0.70, 0.30	0.212	0.204	0.529	0.181
0.65, 0.25	0.192	0.186	0.452	0.152
0.60, 0.20	0.172	0.168	0.388	0.132
0.40, 0.00	0.107	0.106	0.220	0.080
0.40, −1.00	0.266	0.232	0.478	0.456
0.02, −0.40	0.046	0.046	0.091	0.068

TABLE II. DDC parameters related to the characteristic fields and unit of energy for azurite (see text).

Couplings J_1, J_3	H_{c1}	H_{c2}	H_{sat}	Energy scale J_2 in meV and T, respectively
0.02, 0.00	4.12×10^{-3}	1.0100	1.0102	4.16 meV≡32.7 T
0.30, 0.00	0.121	1.143	1.200	3.50 meV≡27.5 T
0.60, 0.00	0.480	1.245	1.500	2.80 meV≡22.0 T
0.80, 0.00	0.795	1.272	1.740	2.41 meV≡19.0 T
0.70, 0.30	0.529	1.390	1.627	2.58 meV≡20.3 T
0.65, 0.25	0.452	1.371	1.569	2.68 meV≡21.0 T
0.60, 0.20	0.388	1.342	1.512	2.78 meV≡21.8 T
0.40, 0.00	0.220	1.183	1.29	3.26 meV≡25.6 T
0.40, −1.00	0.478	0.861	1.234	3.40 meV≡26.7 T
0.02, −0.40	0.091	0.824	0.868	4.84 meV≡38.0 T

which is relevant for an application of the numerical results to azurite. Using the experimental number $H_{sat}=33$ T, the value of the coupling J_2 is calculated from Eq. (2) and the values given in Table II (in both meV and T) may serve to obtain energies and fields applying to azurite in standard units. In Tables I and II, three regimes of the SF phase are covered: (a) values along the $J_3=0$ axis (i.e., for the Heisenberg trimer model), (b) values along a diagonal path which appears as the most interesting one for discussing azurite, and (c) two examples for ferromagnetic coupling. We will discuss below the possibility of such an interaction from the point of view of inelastic excitations. Values along the line $J_1=0.6$, passing through the phase transition at $J_3\approx 0.364$, will be presented in Sec. IV.

If the mapping to an effective low energy Heisenberg chain were perfect, it would imply relations between three different quantities, which are all determined by J_{eff}:

(i) The maximum of the effective one spinon dispersion at wave vector $\pi/2$: $\epsilon(\pi/2)=\pi/2J_{eff}$.

(ii) The critical field which determines the beginning of the plateau: $H_{c1}=2J_{eff}$.

(iii) The width of the effective inverted ferromagnon as the lowest excitation at the beginning of the plateau (in fact, its minimum defines H_{c1}): $\epsilon_{fm}(0)-\epsilon_{fm}(\pi)=2J_{eff}$. This is automatically equal to (ii) from the definition of H_{c1}, but the cosine dispersion is an additional independent property. Since the mapping is only approximate, these quantities differ as is seen in the numerical data and the differences characterize the quality of the mapping. Actually, there are more possibilities to extract J_{eff} from the numerical data such as the energy of the lowest spinon singlet at $k=\pi$ and the ground state energy (suitably extracted from the energy of the saturated subsystem state), but numbers from these approaches essentially confirm the picture as it has emerged from the tables above. The essential conclusion for the real DDC is that the effective coupling J_{eff} depends on energy.

The quantities in Tables I and II have been calculated for $N=24$, but a comparison with results for $N=12$ and $N=18$ shows that finite size effects are very small, indeed negligible to the accuracy given. This is due to the fact that, e.g., J_{eff} is determined by comparing two finite systems, the HAF chain with $N=8$ and the DDC with $N=24$. This is illustrated in Fig. 5, where the excited dimer bands for two different sets of couplings are shown combining results for $N=24$ and $N=18$ in the same graph. We conclude that the effective parameters considered so far can be reliably determined for the infinite chain. The situation is different for the last quantity of interest: the dynamics of the one dimer excitations for $H=0$. These excitations originate by exciting one dimer from singlet to triplet on top of the spinon continuum of the effective HAF chain (instead of on top of the saturated effective HAF chain for Δ_{dimer} as given above). In the following, we give results on this zero field branch as far as numerically possible:

At zero field, the excited dimer states form a continuum as well and the infinite chain limit can only be obtained by extrapolation in $1/N$. With $N=12$ and $N=18$ as the only available numbers of spins, the extrapolation can only be done for wave vectors $k=0$ and $k=\pi$. The lowest energy levels in our finite systems result from coupling of spinons at

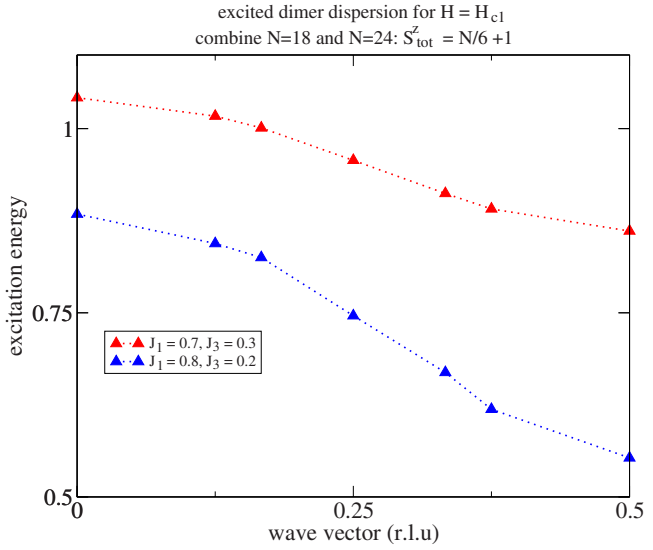

FIG. 5. (Color online) Excited dimer band of the DDC ($N=24$ and $N=18$) above the 1/3 plateau ground state (in a magnetic field H_{c1}) for $J_1=0.7$, $J_3=0.3$ and $J_1=0.8$, $J_3=0.2$.

wave vectors 0 (singlet only) and π (singlet and triplet) to the dimer triplet, i.e., we get a band of one singlet, three triplets, and one quintuplet. However, the separation both between these multiplets and to the higher levels is due to the finite size, whereas in the thermodynamic limit, a continuum with energy of the order of J_2 will result. This is to some extent reflected in the results of finite size extrapolation of the multiplet energies related to one excited dimer: There is a clear tendency for the energies to converge to the same value. Thus, only one energy in this high energy subspace can be given reliably: no reliable information can be obtained in this approach about splitting into bands. In Table III, we give the energy of the lowest state in the continuum of excited dimers obtained this way for a number of coupling constants.

III. DYNAMICS IN THE DIMER-TETRAMER PHASE

The ground state in the tetramer-dimer phase is twofold degenerate and develops from the ground state on the symmetry line $J_1=J_3$. On this line, the two ground states can be written down explicitly (even for finite systems with an ar-

TABLE III. Energies $\epsilon(k=0)$ and $\epsilon(k=\pi)$ in the DDC lowest excited dimer band (onset of the continuum). Values are extrapolated from $N=12$ and $N=18$ to infinite N.

Couplings J_1, J_3	$\epsilon^{dimer}(k=0)$	$\epsilon^{dimer}(k=\pi)$
0.30, 0.00	0.861	0.893
0.60, 0.05	0.988	0.978
0.60, 0.25	0.720	0.711
0.65, 0.25	0.854	0.793
0.70, 0.30	0.864	0.776
0.40, −1.00	1.226	1.255

bitrary even number of cells of three spins). They are given by the alternating sequence of the dimer singlet **S** and the lowest tetramer singlet **T**. This allows the two equivalent configurations

$$\cdots \mathbf{S}\ \mathbf{T}\ \mathbf{S}\ \mathbf{T}\ \mathbf{S}\ \mathbf{T} \cdots$$

and

$$\cdots \mathbf{T}\ \mathbf{S}\ \mathbf{T}\ \mathbf{S}\ \mathbf{T}\ \mathbf{S} \cdots \tag{10}$$

describing the two degenerate ground states.

The lowest excitations above these ground states are obtained as solitons which are defined by gluing together the two degenerate ground states in a localized region on the chain. This gives, e.g., the state

$$\cdots \mathbf{S}\ \mathbf{T}\ \mathbf{S}\ *\ \mathbf{S}\ \mathbf{T} \cdots, \tag{11}$$

where $*$ denotes a free spin. A soliton is possible only with two dimer singlets adjacent to each other and a free spin between them whereas the configuration $\cdots \mathbf{T}\ \mathbf{T} \cdots$ obviously does not exist. On the symmetry line $J_1 = J_3$, there are $N/3$ degenerate localized one-soliton configurations. They start to propagate and to form a soliton band for $J_1 \neq J_3$. The properties of a single soliton can suitably be investigated for chains with an odd number of cells $N/3$ when periodic boundary conditions require the existence of one soliton in the ground state. The hopping process

$$\mathbf{T}\ \mathbf{S}\ * \ \rightarrow\ * \ \mathbf{S}\ \mathbf{T} \tag{12}$$

with amplitude t leads to the propagation of solitons and the formation of a ground state band with energy

$$\epsilon^{\mathrm{sol}}(k) = E_0 + 2t \cos 2k. \tag{13}$$

Thus, from numerical calculations for an odd number of cells, the hopping amplitude is easily determined even when only small systems are available. For infinite chains with periodic boundary conditions and an even number of cells $N/3$ which possess two degenerate ground states and enforce an even number of solitons, the low energy spectrum is dominated by the two soliton continuum emerging from independent propagation of two-solitons with wave vectors $\frac{1}{2}k + k_1$ and $\frac{1}{2}k - k_1$, i.e.,

$$\epsilon^{2\mathrm{sol}}(k) = 2E_0 + 4t \cos k \cos 2k_1. \tag{14}$$

Numerically obtained soliton spectra are shown in Fig. 6 for (a) $N=15$ and (b) $N=18$ for the point $J_1=0.6, J_3=0.55$ close to the symmetry line in the phase diagram. $\epsilon^{\mathrm{sol}}(k)$ in Fig. 6(a) clearly shows the $\cos 2k$ dispersion, whereas the dispersion of $\epsilon^{2\mathrm{sol}}(k)$ in Fig. 6(b) is somewhat more complicated due to the small size of the system. Also shown are the three- and four-soliton bands, respectively, demonstrating the clear division of the spectra into distinct soliton bands for this nearly symmetric set of couplings [the zero of energy in Fig. 6(a) is taken from the noninteracting limit]. The situation is analogous to the Ising chain with small transverse interactions, the system where the dynamics of magnetic solitons was discussed first.[15,16] Slightly different, the soliton spin 1/2 here is a real spin 1/2 which can be attributed to the free electron of the Cu^{2+} ion between the two dimers forming

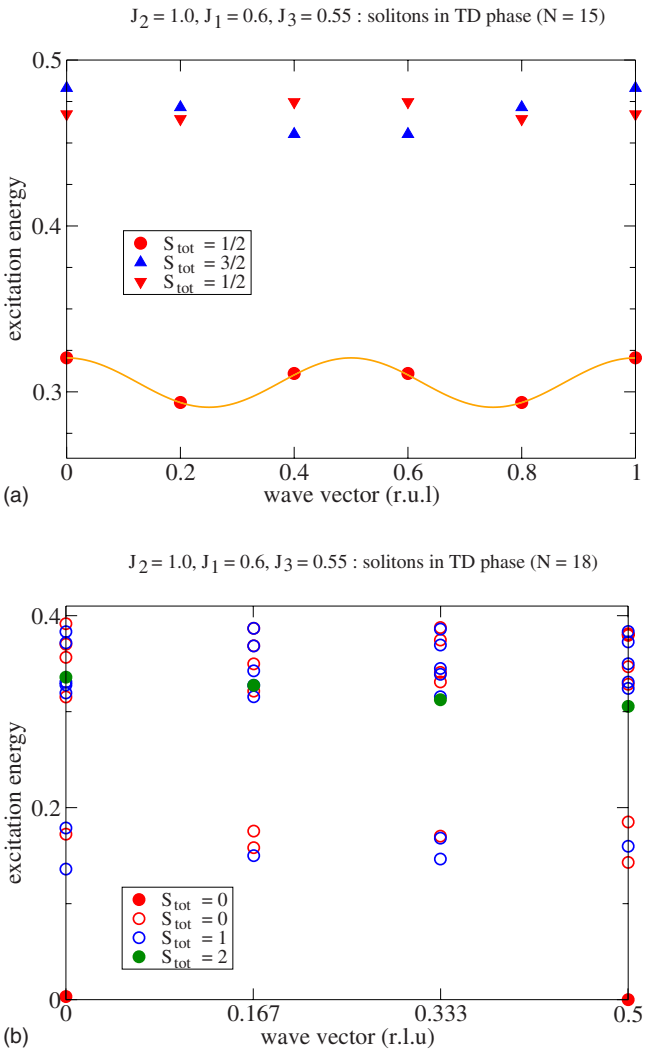

FIG. 6. (Color online) Soliton spectrum of the DDC [(a) $N=15$, (b) $N=18$] in the TD phase for $J_1=0.6, J_3=0.55$. The $N=15$ spectrum is shown in the complete Brillouin zone $k=0,\ldots,2\pi$ to demonstrate the $\cos 2k$ dispersion of the single soliton.

the domain wall. For small numbers $N/3$, the soliton spectrum clearly shows the effects of the different symmetries of the singlet and triplet.

From the one-soliton data for $N=15$ and $J_1=0.6, J_3=0.55$, the hopping amplitude is deduced as $t \approx 0.0076$. For the two-soliton data for $N=18$, the corresponding calculation has to include the possibility of two neighboring solitons as well as the resulting symmetry effects and gives a somewhat higher value, $t \approx 0.0097$. The deformation of the zero order wave function due to neighboring solitons is strongest for small systems, which explains the difference. However, for $N=24$ (when only the lowest two-soliton band is accessible in Lanczos calculations), we obtain $t \approx 0.0076 \pm 0.0002$, identical to the one-soliton result for $N=15$ within the uncertainty resulting from matching the cosine dispersion for the different wave vectors.

IV. CROSSING THE PHASE TRANSITION LINE

In this section, we present some data for the specific heat and for the spectrum of low-lying excitations in order to

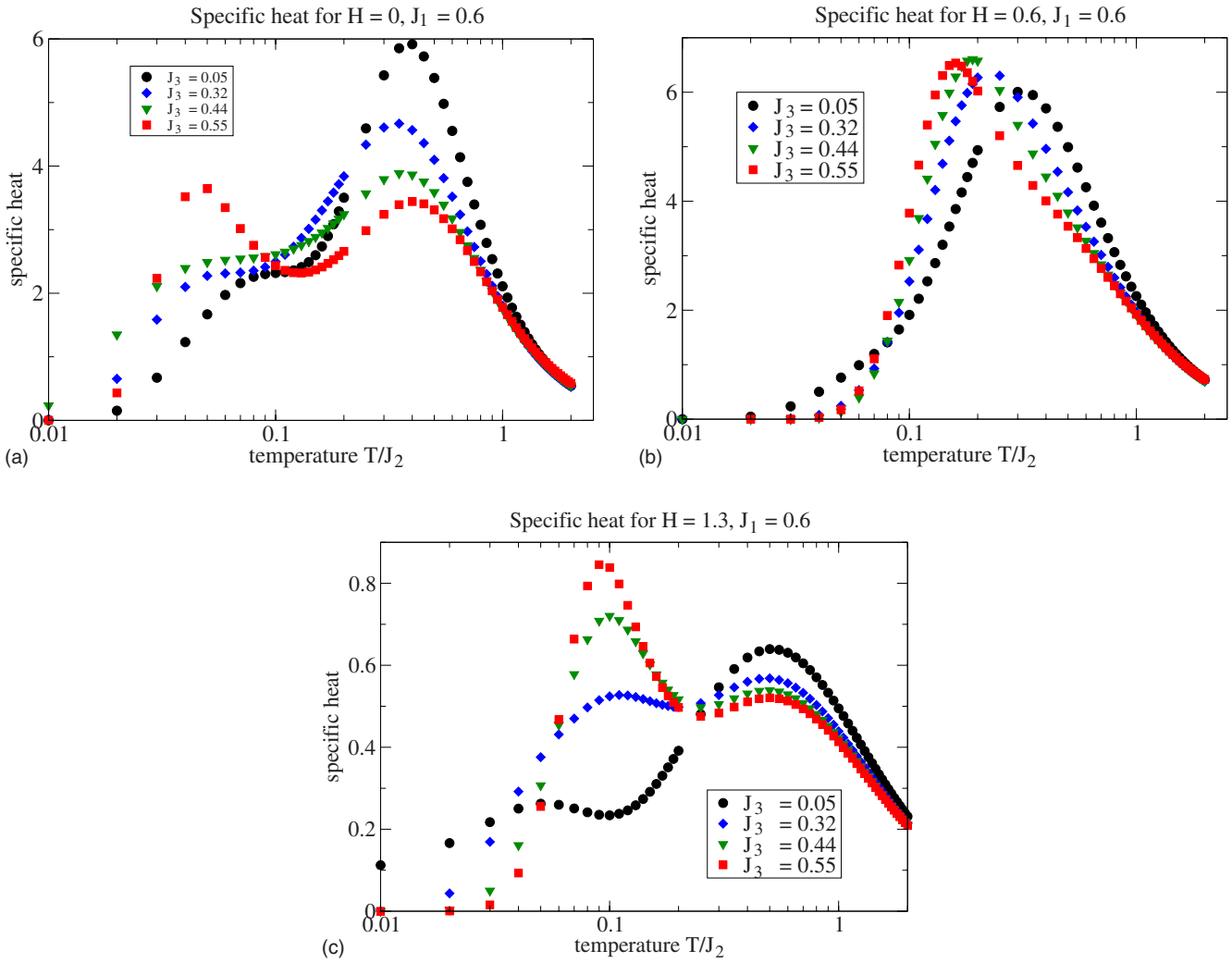

FIG. 7. (Color online) Specific heat of the DDC (from all levels for $N=18$) for (a) $H=0$, (b) $H=0.6$, and (c) $H=1.3$, fixed $J_1=0.6$ and varying J_3 through the phase transition.

approach the behavior of the system when its coupling constants change between well defined end points, one in the SF phase, and the other one in the TD phase, thus crossing the phase transition line. Evidently, owing to the small system sizes accessible only in our calculations, we cannot claim that these data describe correctly the most interesting aspect, namely, the critical behavior; on the other hand, our data for both the specific heat and the spectrum of low-lying excitations set a reasonable frame for the transition regime, to be filled by more detailed calculations later. In the following, we present results for the DDC on the line $J_2=0.6$ for varying J_3. As discussed above, the phase transition along this line is of Kosterlitz-Thouless type and can be considered as a generalization of the phase transition in the HAF with both nearest and next-nearest neighbor exchanges. We therefore have applied the procedure of Ref. 11 to determine the critical coupling and found that the phase transition occurs at $J_3 \approx 0.364$.

Figure 7 shows a sequence of specific heat data varying J_3 for fixed J_1 for three different values of the magnetic field. The data are obtained from the full spectrum for the $N=18$ chain and therefore reliably cover the complete temperature regime although critical properties near the critical coupling $J_3 \approx 0.364$ will appear smeared out. In all the diagrams, we use a logarithmic temperature scale adequate to the strongly different energy scales. For all magnetic fields, the specific heat exhibits a high temperature peak at $T \approx 0.5$, whereas the low temperature properties reflect the structure of the system. For $H=0$ and low temperature [Fig. 7(a)], the SF phase is characterized by a continuously increasing contribution to the specific heat, the remnant of the effective Luttinger liquid. With increasing J_3, this contribution develops gradually into the gapped contribution of the TD phase with characteristic shoulders on both sides of the phase transition at $J_3 \approx 0.364$. For $H=0.6$ [Fig. 7(b)], the DDC is always in the gapped plateau regime and the specific heat shows little variation with the coupling. For $H=1.3$ [Fig. 7(c)], the DDC is close to saturation and the differences between the two phases, resulting from the energy spectra above the plateau gap, become apparent again. In particular, the well defined grouping into soliton bands at $J_3=0.55$ leads to a strong low temperature peak which actually develops continuously from lower J_3 values. It would be interesting to see, using more powerful numerical methods, whether the development of

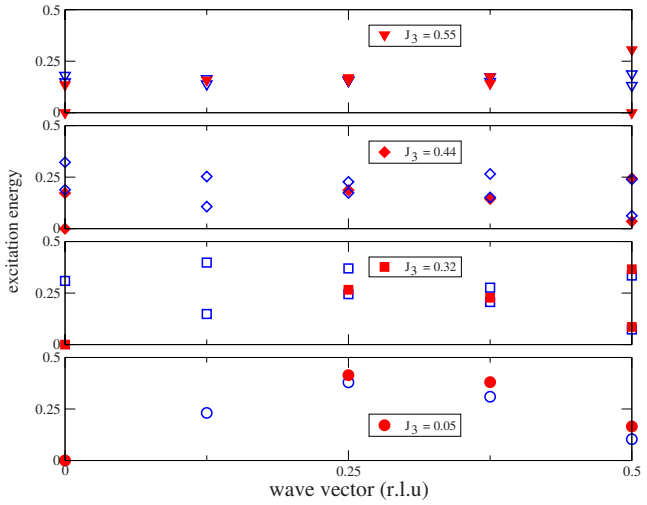

FIG. 8. (Color online) Low-lying spectra [$S_{\mathrm{tot}}=0$ (red/full) and $S_{\mathrm{tot}}=1$ (blue/open)] of the DDC ($N=24$) for $J_1=0.6$ and $J_3=0.55,0.44,0.32,0.05$.

this peak in the nearly saturated case shows critical properties. Whereas the qualitative behavior of the specific heat for $H=0$ and $J_1=0.6$, $J_3=0.32$ agrees with the experimental data for azurite shown in Ref. 9, a detailed comparison for an appropriate parameter set requires data with the necessary subtraction of the phonon contribution.

Figure 8 shows a sequence of spectra of low-lying excitations ($S_{\mathrm{tot}}=0,1$) in a zero magnetic field obtained by the same procedure as the spectra shown in Secs. II and III. Qualitatively, the transition from the SF phase with its gapless spinon continuum to the gapped soliton spectra in the TD phase is clearly seen, as far as possible for the limited size of the system. With increasing J_3, the second degenerate ground state at $k=\pi$ emerges, the spinon continuum deforms into the soliton band, and the gapless character disappears. Excitation spectra in a finite magnetic field, in particular, for fields in the plateau regime, on the other hand, do not show specific variations but rather continuous changes across the phase diagram without prominent features close to $J_3=0.364$, the location of the phase transition in zero field. This illustrates, as expected, that the signature of the phase transition in the dynamics is limited to zero external field and low-lying excitations, whereas the $1/3$ plateau as well as the accompanying high energy excitations are continuous across the phase diagram.

V. CONCLUSIONS

For the $S=1/2$ distorted diamond chain in both the SF and the TD phases, we have calculated the spectra of low-lying excitations and the specific heat. We have used both full numerical diagonalization (for chains with up to 18 spins) and the Lanczos algorithm (for chains with up to 24 spins) and have discussed the results in relation to approximate analytic approaches. Except close to the SF-TD phase transition, results for our small systems are shown to represent the thermodynamic limit. Our calculations are for an arbitrary value of the external magnetic field. Results are mainly given for zero field and for fields corresponding to the $1/3$ plateau regime.

In the SF phase, the low energy spectra can be related to a Heisenberg antiferromagnetic chain with effective interaction J_{eff}. For parameters beyond the validity of a perturbative approach, this effective interaction has to be allowed to be energy dependent. The lowest excitations in the plateau regime are the inverted ferromagnon and the propagating single dimer triplet excitation with, however, partly strong modifications of the corresponding cosine dispersions. The values of the characteristic parameters (J_{eff}, extent of the plateau regime, widths of the cosine bands) are given for typical paths crossing the SF phase. These data should allow to decide whether a material such as $Cu_3(CO_3)_2(OH)_2$ (azurite) is sufficiently well described by the DDC model and, if so, to determine the corresponding couplings. The standard assumption for azurite is to take all couplings as antiferromagnetic and we have shown that the spectra of low-lying excitations exhibit large and characteristic changes when the possibility of one ferromagnetic coupling is introduced. We therefore expect that our data will allow us to interpret quantitatively experimental data on azurite. This refers, in particular, to the results of inelastic neutron scattering experiments.[10] Considering the present status of such investigations, our results do not confirm the conclusion of at least one ferromagnetic coupling in azurite. This is in agreement with previous conclusions based on the specific heat in Ref. 9 and also, using the xy version of the model, in Ref. 13.

Our results lead us to describe the following signatures of the DDC when ferromagnetic couplings are present:

(i) Whereas the dimer width is roughly $1/2$ of the ferromagnon width for antiferromagnetic couplings (as suggested by perturbation theory), for ferromagnetic couplings, these widths tend to become equal.

(ii) The sign of the couplings has a marked influence on the relative appearance of the ferromagnon and the excited dimer band. For couplings $J_1,J_3=(-1,0.4)$, these bands above the $1/3$ plateau overlap, whereas for $(-0.4,0.02)$, ferromagnon as well as dimer width become very small and, correspondingly, H_{c1} becomes much smaller than in perturbation theory.

The low-lying excitations in the TD phase with its twofold degenerate ground state are shown to be solitons. The width of the one-soliton band as determined from the $N=15$ chain not too far from the symmetry line $J_1=J_3$ reproduces well the soliton bands in the $N=24$ chain and therefore gives reliably the tunneling amplitude for the soliton propagation in the thermodynamic limit.

We have also shown spectra as well as the specific heat on a line across the SF-TD phase transition. Although the small systems accessible to us do not allow us to discuss critical properties of the DDC close to this Kosterlitz-Thouless transition, the variation of the dynamical properties through the transition becomes clear. In particular, only the low energy properties, determining the behavior of the system at zero field, carry the signature of the phase transition.

Generally, the DDC has many features in common with the antiferromagnetic Heisenberg chain with nearest and next-nearest exchange and the SF-TD phase transition is of

the same type as the Kosterlitz-Thouless transition at $J_{\mathrm{NNN}}=0.2411,\ldots,J_{\mathrm{NN}}$ in this system. On the other hand, we have shown that the additional degrees of freedom, resulting from the possibility to excite the J_2 dimers to the triplet state, show up clearly in the dynamics. We leave the investigation of the influence of these degrees of freedom on the phase transition using more powerful analytical and numerical methods to the future.

ACKNOWLEDGMENTS

We wish to thank H. Ohta, H. Kikuchi, K. Rule, S. Süllow, and D. A. Tennant for stimulating discussions. We gratefully acknowledge that computational facilities for the numerical calculations were generously provided by the John von Neumann Institut for Computing at Jülich Research Center.

[1] K. Takano, K. Kubo, and H. Sakamoto, J. Phys.: Condens. Matter **8**, 6405 (1996).
[2] K. Okamoto, T. Tonegawa, Y. Takahashi, and M. Kaburagi, J. Phys.: Condens. Matter **11**, 10485 (1999).
[3] T. Tonegawa, K. Okamoto, T. Hikihara, Y. Takahashi, and M. Kaburagi, J. Phys. Soc. Jpn. **69**, 332 (2000).
[4] A. Honecker and A. Läuchli, Phys. Rev. B **63**, 174407 (2001).
[5] K. Okamoto, T. Tonegawa, and M. Kaburagi, J. Phys.: Condens. Matter **15**, 5979 (2003).
[6] B. Gu and G. Su, Phys. Rev. Lett. **97**, 089701 (2006).
[7] B. Gu and G. Su, Phys. Rev. B **75**, 174437 (2007).
[8] H. Ohta, S. Okubo, T. Kamikawa, T. Kunimoto, Y. Inagaki, H. Kikuchi, T. Saito, M. Azuma, and M. Takano, J. Phys. Soc. Jpn. **72**, 2464 (2003); S. Okubo, A. Taketani, H. Ohta, T. Kunimoto, Y. Inagaki, T. Saito, M. Azuma, M. Takano, and H. Kikuchi, Prog. Theor. Phys. Suppl. **159**, 11 (2005).
[9] H. Kikuchi, Y. Fujii, M. Chiba, S. Mitsudo, T. Idehara, T. Tonegawa, K. Okamoto, T. Sakai, T. Kuwai, and H. Ohta, Phys. Rev. Lett. **94**, 227201 (2005); **97**, 089702 (2006); B. Gu and G. Su, *ibid.* **97**, 089701 (2006).
[10] K. C. Rule, A. U. B. Wolter, S. Süllow, D. A. Tennant, A. Brühl, S. Köhler, B. Wolf, M. Lang, and J. Schreuer, arXiv:0709.2560 (unpublished).
[11] K. Okamoto and K. Nomura, Phys. Lett. A **169**, 433 (1992).
[12] S. Chen, Y. Wang, W. Ning, C. Wu, and H. Lin, Phys. Rev. B **74**, 174424 (2006).
[13] H. H. Fu, K. L. Yao, and Z. L. Liu, Phys. Rev. B **73**, 104454 (2006).
[14] A. Honecker (unpublished).
[15] J. Villain, Physica B & C **79**, 1 (1975).
[16] N. Ishimura and H. Shiba, Prog. Theor. Phys. **63**, 743 (1980).